Exploration case studies in mature Gulf of Mexico basins using 3D marine CSEM

H. Yuan (hyuan@emgs.com), T. Pham (pham@emgs.com), J.J. Zach (jjz@emgs.com), M.A. Frenkel (maf@emgs.com), and D. Ridyard (dr@emgs.com) / EMGS ASA*

Summary

High salt concentrations and small targets in complicated geology often found in the Gulf of Mexico have been an impediment to the application of marine CSEM techniques, until recent advances in operations, acquisition hardware and advanced processing techniques permit 3D-mapping of complex resistivity distributions. Using two examples from a recent pre-lease sale campaign, we demonstrate the successful application of the entire value chain from customized acquisition grids, multi-frequency acquisition to processing of data including wide-azimuth lines with reliable phase and amplitude, and subsequent inversion-based 3D interpretation. Advanced interpretation is based on an iterative Hessian-based inversion with quasi-Newton update and fast finite-difference time-domain modeling. Inversion results are used to construct resistivity distribution consistent with 3D-seismic images. During the campaign, we successfully addressed the client's need to resolve small targets (2 km x 2 km) with low-resistivity pay ($\Delta\rho < 5$ Ωm), many found in the vicinity (<1 km) of large salt bodies.

Introduction

Marine controlled-source electromagnetic (CSEM) methods for hydrocarbon detection relying on a horizontal electric bipole (HED) emitting a predefined low frequency spectrum (0.05-10 Hz), and the recorded electromagnetic fields by ocean bottom receivers, have been used in hydrocarbon exploration on a commercial scale since 2002 (Eidesmo et al., 2002). The sensitivity to hydrocarbons is due to the relative enhancement of the transverse magnetic component of the received electromagnetic signal through a partial waveguide effect by buried resistors, which can be either hydrocarbon deposits or other resistive bodies.

Marine CSEM has become a method for 3D imaging of areas with complex geologies, which is applied by many major oil companies, either as a stand-alone frontier exploration tool (Monk et al., 2008; Suffert et al., 2008) or in conjunction with, or addition to other geophysical probes. Recent published case studies for the latter include Carrazone et al. (2008), Price et al. (2008) Plessix and van der Sman (2008), Zach and Frenkel (2009), and Zach et al.(2009).

Advances in hardware and operations have resulted in a vast improvement in data quality, permitting the acquisition of well-defined and repeatable grids of seabed receivers with complex towing patterns including the acquisition of wide-azimuth data with consistent magnitude and phase (Zach et al., 2008b). Such high-fidelity physical measurements enable the effective use of 3D inversion techniques. They allow for imaging of multiple resistive bodies in the subsurface. The majority of 3D CSEM inversion techniques rely on iterative optimization where the gradient of a misfit functional with respect to a discrete conductivity grid is computed during each iteration. The present approach employs the quasi-Newton method described in Zach et al. (2008a). It is based on the gradient calculation developed by Støren et al. (2008) and the fast finite-difference time-domain modeling code by Maaø (2007). Other notable recent contributions to CSEM inversion methodology include Commer and Newman (2008) on joint CSEM and MT inversion, Jing et al. (2008), which shows the importance of anisotropy in many surveys, as well as Norman et al. (2008) for joint interpretation with seismic data (see also additional references in Zach et al. (2008a)).

The high resistivities in geologic salt deposits, as well as relatively small targets typically found in a mature area such as the Western Gulf of Mexico (GoM) have caused only reluctant adoption of marine CSEM in the GoM. However, we demonstrate that with properly designed surveys and thorough inversion-based 3D interpretation, where resistors from inversion resistivity cubes are remapped into seismic containers, this challenge can be successfully addressed.

Description of fields

EMGS was approached by Focus Exploration, LLC, a Gulf of Mexico prospect generation company, to evaluate several prospects in the Western GoM. All prospects are located above or near salt with varying other geologic complexities. Two representative examples are shown here:

1) A 1980's exploration well drilled in about 1 km of water (Figure 1) resulted in only one of the targeted prospects bearing hydrocarbons, rendering the find non-commercial. With improved deviated drilling capabilities and a higher oil price, the decision was made to test possible down-dip pay a few km away from the original well. Due to large and complicated salt deposits, and all prospects located beneath shale distributions with complex local resistivity distribution, a dense 3D CSEM receiver grid was used.

2) The second survey area represents a more complex geological setting with several major faults extended to the

near surface and a salt dome nearby (Figure 2). Two wells were drilled in this area: Well A in the east with ~85 ft gas pay at around 1000 m BML, and well B in the south with no significant find (see Figure 7 for a map view). A CSEM survey was acquired to evaluate an up-thrown channel target that was identified from seismic data by Focus Exploration. The prospect is ~1.5x2.2 km located at ~700 m BML. The survey consists of three parallel lines and one crossing line as shown in Figure 7.

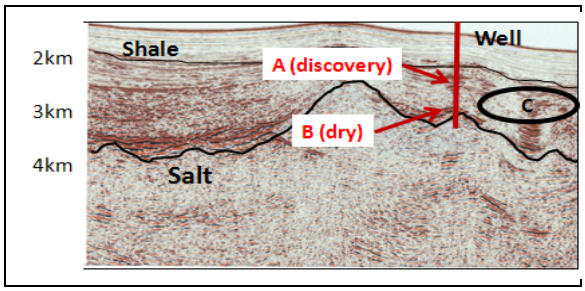

Figure 1: Survey 1: seismic image and location of 1980's exploration well through prospects A and B, Western Gulf of Mexico. C shows the location of possible down-dip pay.

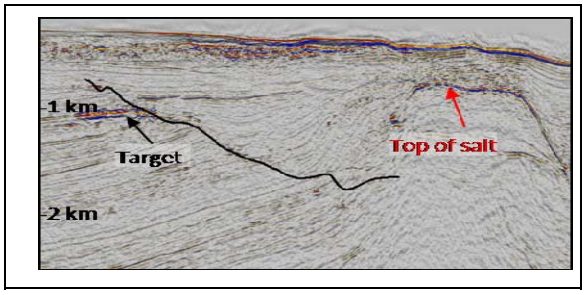

Figure 2: Survey 2: up-thrown target shows strong amplitude on seismic. Salt dome is present but beyond the receiver drop range.

3D acquisition and advanced processing

The overall workflow for inversion-based 3D interpretation is shown in Figure 3. Receiver data, such as from the grid shown in Figure 4, is conditioned for 3D inversion, producing frequency-domain data and noise estimates using the methodology described in Zach et al. (2008b). The noise estimates are used to determine the data weights for inversion, where a binary weighting scheme is employed with a SNR-cutoff of 24 dB. After receiver orientations are determined from a data-drive approach, the full vector field can be recovered to within 5% in magnitude and 5 degrees in phase. The starting model for full 3D inversion is prepared using accurate seafloor data from seismic (if available) or other surveys, the measured resistivity of the water column and an initial estimate for the subsurface resistivity distribution. The latter is obtained using global-search plane-layer inversions (Roth and Zach, 2007) of the inline electric and transverse magnetic field from several or all receivers to identify general trends and to determine a starting model. Likely resistive boundaries can thereby be imported from seismic horizons. However, due to a superior signal-to-noise ratio, only electric data are used in the full 3D inversion. The full turn-around time for 3D inversion for a given starting model is typically 80-200 iterations (about 1 week on 150 parallel nodes). For details of the algorithm, see Zach et al.(2008a). If high-quality seismic data are available, as was the case for all prospects in the present GoM campaign, results from 3D inversion are compared with seismic images, and the resulting resistivity cubes from inversion are mapped into seismic "containers", while preserving the same transverse resistance $R_t=(\Delta\rho)(\Delta z)$. Forward modeling is then conducted with the resulting geological model, and if the resulting synthetic data show discrepancies with measured data, the mapping from the inversion results is modified. For severe discrepancies, the entire inversion needs to be repeated with a different starting model or optimization parameters.

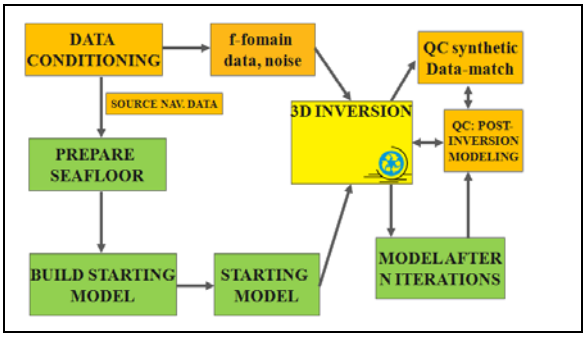

Figure 3: Workflow for inversion-based 3D interpretation of marine CSEM data.

Case study 1:

From the dataset shown in Figure 4, acquired with four main source modes (0.25, 0.5, 0.75, and 1.0 Hz), inline and

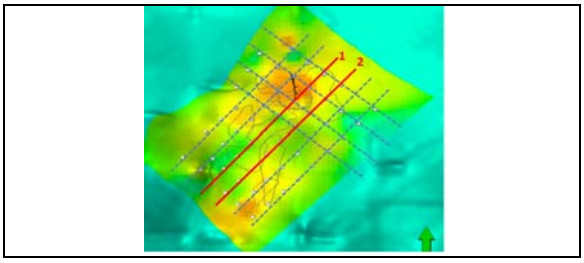

Figure 4: Survey layout of case study 1 (receiver drops in white, blue dashes and red solid lines: towlines), along with 3D-inversion resistivity map at the TVD=1800m-level.

azimuthal horizontal electric data for each receiver were inverted. The best data fit was achieved with a complex starting model derived from plane-layer inversions on a subset of individual receivers.

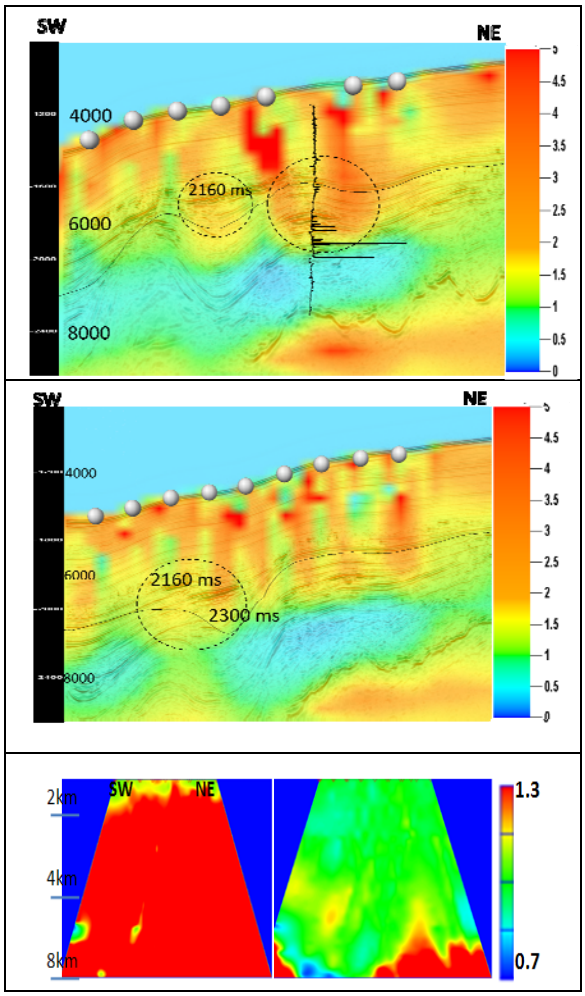

Figure 5: Final result from 3D inversion of case study 1. Top/center panel: resistivity profile along lines 1 and 2 (Figure 4), along with the proven hydrocarbon find (well log) and locations of additional down-dip pay (2160 ms, 2300 ms). Bottom left/right panel: representative misfit plot for initial/final model, line 2 from Figure 4; shown: normalized magnitude for 0.5 Hz real versus synthetic data.

The projection of the resulting resistivity cube from 3D-inversion on two representative lines is shown in Figure 5. The bulk resistivity in the known stacked pay is confirmed in its cumulative response, while the depth separation (<75 m) is just under the vertical spatial resolution. The geologic noise at shallow depths is due to shale-microstructure. Overall, the known geology of the area, including shale resistivity, salt horizons and the brine-saturated sandstone beneath the shale is confirmed. The prospect is clearly delineated and possible previously bypassed down-dip pay is identified towards the Southwest of the original find. The subsequent post-inversion 3D-modeling is demonstrated in Figure 6 (only showing a 2D-projection of the 3D-model used), which shows equivalent resistors to the 3D-inversion results consistent with possible containers found from seismic images, again requiring additional thin resistors to the proven ones to minimize the misfit between real and synthetic data.

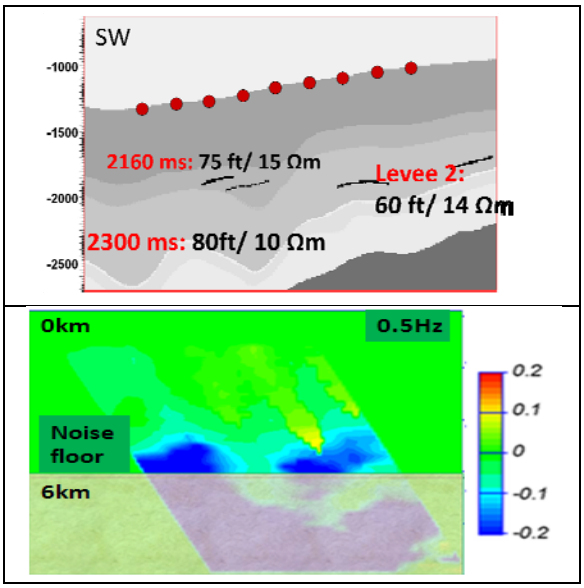

Figure 6: Post-inversion 3D modeling: cross section along line 2 (Figure 4). Top: equivalent resistivities to bulk resistivity from the 3D inversion cube consistent with seismic containers, showing possible additional bypassed down-dip pay on the SW-side. Bottom: misfit plot for inferred model (nMVO at f=0.5 Hz).

Case study 2:

A semi-grid CSEM survey with three parallel lines and one crossing line was acquired over the prospect of the second field (Figure 7). Inversion was run for all four lines with 0.25 Hz. The starting model was created utilizing the resistivity log of well B as well as the plane-layer inversion results of several receivers. Seismic horizons were also used in the starting model as layer boundary constrain. The inverted resistivity along the NW-SE line is superimposed on seismic and shown in the top panel of Figure 8. The discovery well A located in the east is successfully confirmed by a resistive body at the correct depth (resistivity log is shown to the right of the well). High resistivity observed at the prospect location proved the client's expectation from seismic interpretation and also

indicated possible extension of the prospect towards west where seismic data are unavailable. The misfit plot of the same line is show in the bottom panel of Figure 8 for starting and final model on the left and right, respectively. The obvious large misfits beyond 4.5 km offset in the final model are due to a noisy receiver. The measure phase data is explained by the final resistivity model to within 5 degree for the majority of the input receiver data.

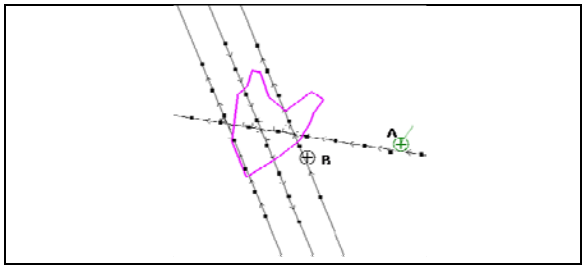

Figure 7: Survey layout for case study 2. Purple is the outline of the prospect to be studied. Receiver drops are denoted as black dots. Crosses indicate positions of wells A and B.

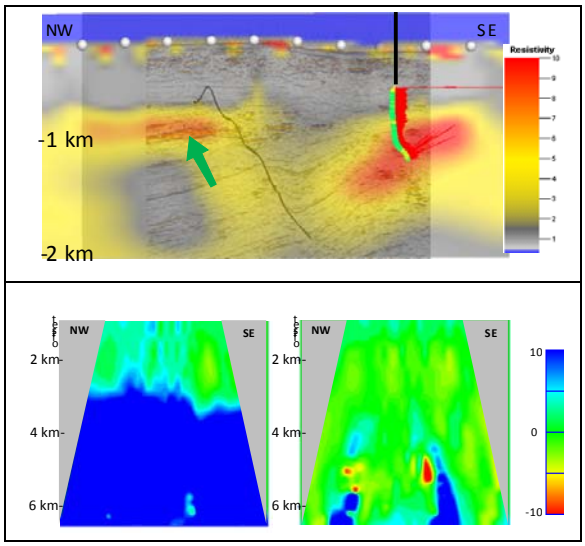

Figure 8: Final result from 3D inversion of case study 2. Top panel: resistivity profile along the NW-SE line in Figure 7, along with the proven hydrocarbon find (SE) and the prospect identified (NW) . Bottom left/right panel: misfit plot for initial/final model of the same line for 0.25 Hz phase data.

Figure 9 shows a depth slice of the resulting resistivity cube from 3D inversion at the prospect depth level (top) and proven discovery level (bottom). A good correlation is shown between the resistive body in the middle of the survey and the prospect outline provided by the client. The found hydrocarbon is confirmed by the inversion results as well.

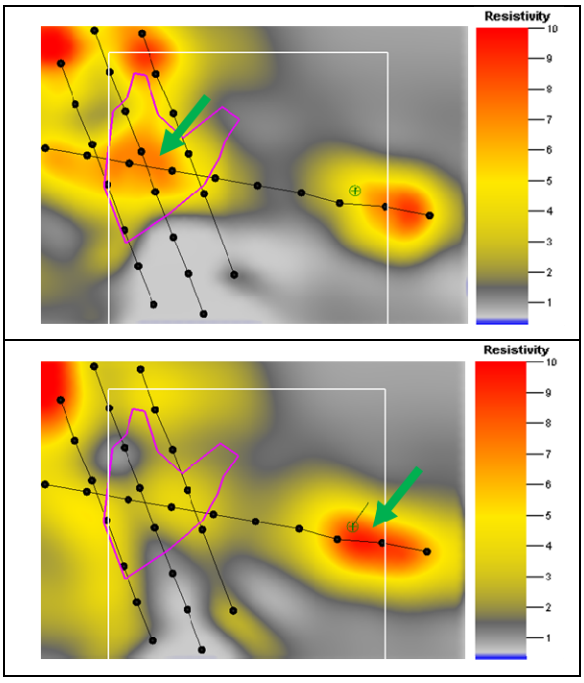

Figure 9: Resistivity depth slice of case study 2 at the prospect level (top) and proven discovery level (bottom).

Conclusions

A case study of two representative fields from a recent 3D-CSEM campaign in the Western GoM was presented. The successful confirmation of drilling results by 3D CSEM imaging in both cases proved the applicability of CSEM technology in the GoM where massive salt and complex geologies are often seen. The state-of-the-art survey design, acquisition and advanced processing allow sufficient data coverage and resolution to recover prospects with sizes around 1.5-2 km, even within a salt province.

Acknowledgements

We would like to express our gratitude towards Donald Crider and Michael Scherrer of Focus Exploration, LLC, for valuable discussions as well as the agreement to show field data. Special thanks go to Bjarte Bruheim for support throughout this study, to Arun Kumar, Anne-Marit Ostvedt-Ghazi, Joanne Suffert, Marianne Jensen and Adekunle Odutola of EMGS for help in preparing the case study section. We further would like to thank EMGS ASA for permitting this publication.

EDITED REFERENCES

Note: This reference list is a copy-edited version of the reference list submitted by the author. Reference lists for the 2009 SEG Technical Program Expanded Abstracts have been copy edited so that references provided with the online metadata for each paper will achieve a high degree of linking to cited sources that appear on the Web.

REFERENCES

Carrazone, J. J., T. A. Dickens, K. E. Green, C. Jing, L. A. Wahrmund, D. E. Willen, M. Commer, and G. A. Newman, 2008, Inversion study of a large marine CSEM survey: 78th Annual International Meeting, SEG, Expanded Abstracts, 644–647.

Commer, M., and Newman, G.A., 2008, Optimal conductivity reconstruction using three-dimensional joint and model-based inversion for controlled-source and magnetotelluric data: 78th Annual International Meeting, SEG, Expanded Abstracts, 609613.

Eidesmo, T., S. Ellingsrud, L. M. MacGregor, S. Constable, M. C. Sinha, S. Johansen, F. N. Kong, and H. Westerdahl, 2002, Sea bed logging (SBL), a new method for remote and direct identification of hydrocarbon filled layers in deepwater areas: First Break, **20**, 144–152.

Jing, C., K. E. Green, and D. E. Willen, 2008, CSEM inversion: Impact of anisotropy, data coverage, and initial models: 78th Annual International Meeting, SEG, Expanded Abstracts, 604–608.

Maaø, F. A., 2007, Fast finite-difference time-domain modeling of marine-subsurface electromagnetic problems: Geophysics, **72**, no. 2, A19–A23.

Monk, D., F. Roth, J. Ross, and C. Twarz, 2008, Application of electromagnetic scanning to an Australian frontier basin with complex bathymetry: OTC Proceedings.

Norman, T., H. Alnes, O. Christensen, J. J. Zach, O. Eiken, and E. Tjåland, 2008, Planning time-lapse CSEM-surveys for joint seismic-EM monitoring of geological carbon-dioxide injection: EAGE CO2 Geological Storage Workshop.

Plessix, R. -E., and P. van der Sman, 2008, Regularized and blocky controlled source electromagnetic inversion: PIERS.

Price, A., P. Turpin, M. Erbetta, D. Watts, and G. Cairns, 2008, 1D, 2D and 3D modeling and inversion of 3D CSEM data offshore West Africa: 78th Annual International Meeting, SEG, Expanded Abstracts, 639–643.

Roth, F., and J. J. Zach, 2007, Inversion of marine CSEM data using up-down wavefield separation and simulated annealing: 77th Annual International Meeting, SEG, Expanded Abstracts, 524–528.

Støren, T., J. J. Zach, and F. Maaø, 2008, Gradient calculations for 3D inversion of CSEM data using a fast finite-difference time-domain modelling code: 70th Annual Conference and Exhibition, EAGE, Extended Abstracts.

Suffert, J., P. Sangvai, F. Roth, A. Tyagi, and R. Bastia, 2008, Frontier exploration by electromagnetic scanning – a deep water example: 78th Annual International Meeting, SEG, Expanded Abstracts, 662–666.

Zach, J. J., A. K. Bjørke, T. Støren, and F. Maaø, 2008a, 3D inversion of marine CSEM data using a fast finite-difference time-domain forward code and approximate Hessian-based optimization: 78th Annual International Meeting, SEG, Expanded Abstracts, 614–618.

Zach, J. J., F. Roth, and H. Yuan, 2008b, Data preprocessing and starting model preparation for 3D inversion of marine CSEM surveys: 70th Annual Conference and Exhibition, EAGE, Extended Abstracts.

Zach, J. J., and M. A. Frenkel, 2009, 3D Inversion-Based Interpretation of Marine CSEM Data: OTC.

Zach, J. J., M. A. Frenkel, A. M. Ostvedt-Ghazi, A. Kumar, T. Pham, 2009, Detecting low-pay reservoirs in salt provinces using 3D inversion of marine CSEM surveys – a Gulf of Mexico case study: 71st Annual Conference and Exhibition, EAGE, Extended Abstracts.